

REPORT DOCUMENTATION PAGE

1. REPORT SECURITY CLASSIFICATION Unclassified	10. RESTRICTIVE MARKINGS
2. SECURITY CLASSIFICATION AUTHORITY	3. DISTRIBUTION/AVAILABILITY OF REPORT Approved for public release; distribution unlimited
3. DECLASSIFICATION/DOWNGRADING SCHEDULE	
4. PERFORMING ORGANIZATION REPORT NUMBER(S) Technical Report # 52	5. MONITORING ORGANIZATION REPORT NUMBER(S)
6. NAME OF PERFORMING ORGANIZATION Dept. of Chemistry George Washington Univ.	6a. NAME OF MONITORING ORGANIZATION Office of Naval Research (Code 413)
6c. ADDRESS (City, State, and ZIP Code) Washington, DC 20052	7a. NAME OF SPONSORING ORGANIZATION (If Applicable)
7. NAME OF SPONSORING ORGANIZATION Office of Naval Research (City, State, and ZIP Code) 800 Nth, Quincy, Arlington, VA 22211	7b. ADDRESS (City, State, and ZIP Code) Chemistry Program 800 N. Quincy Street Arlington, VA 22217
7c. TITLE (Include Security Classification) Understanding Electronegativity Effects in Core-Level Electron Spectroscopies: Application to the High-Temperature Superconductors	7c. ADDRESS (City, State, and ZIP Code) Contract N00014-89-J-1103
8. PERSONAL AUTHORITY D. E. Ramaker	8. PROCUREMENT INSTRUMENT IDENTIFICATION NUMBER Contract N00014-89-J-1103
9. TYPE OF REPORT Interim Technical	9. SOURCE OF FUNDING NUMBERS PROGRAM ELEMENT NO.
10. TIME COVERED From To	10. SOURCE OF FUNDING NUMBERS PROJECT NO.
11. DATE OF REPORT (Month/Year) December 1989	11. DATE OF REPORT (Month/Year) 17
12. SUPPLEMENTARY NOTATION Prepared for Publication In	12. SUBJECT TERMS (Continue on reverse if necessary and identify by block number) Electronegativity Effects, Transition metal oxides, High Temp. superconductors, Photoelectron spectra
13. ABSTRACT (Continue on reverse if necessary and identify by block number) The nature of the core level reflected in x-ray photoelectron spectroscopy, Auger electron spectroscopy, and x-ray absorption near edge structure is considered. An understanding of the effects of anion and cation electronegativity on spectra for the transition metal halides is obtained. This knowledge is applied to understand similar spectra for the high temperature superconductors.	14. ABSTRACT SECURITY CLASSIFICATION Unclassified
15. JOURNAL OF ELECTRON SPECTROSCOPY AND RELATED PHENOMENA Journal of Electron Spectroscopy and Related Phenomena	16. TELEPHONE NUMBER (Area Code) 202-696-4410
17. GEORGE WASHINGTON UNIVERSITY Department of Chemistry Washington, D.C. 20052	17b. OFFICE SYMBOL SECURITY CLASSIFICATION OF THIS PAGE Unclassified
18. DECEMBER 1989	18a. APRIL 1990 All other editions are obsolete.

Reproduction in whole, or in part, is permitted for any purpose
of the United States Government.

* This document has been approved for public release and sale;
its distribution is unlimited.

DTIC
SELECTED
JAN 11 1990
S B C2 D

AD-A216 728

90 01 10 162

2. THE CORE-LEVEL IN XPS

2.1 The Nature of the Satellites

The metal 2p XPS data for TM compounds generally exhibit a main peak plus one or two satellite peaks at higher binding energy (5-14). Figure 1 summarizes the energy separation, ΔE , between the main and satellite peaks, and Fig. 2 shows XPS data for titanium and copper halides (7,12); examples at the left and right sides of the TM series. Several mechanisms have been proposed to explain the origin of these satellites (15). The models involving charge transfer (CT) seem to be gaining the most acceptance for explaining at least some of the 2p core level satellites (7,8,10). A different mechanism, the excitonic satellite mechanism (19), appears to be the most promising for explaining the satellites at larger energy separation. Fig. 1 distinguishes between those features identified as charge transfer and excitonic

UNDERSTANDING ELECTRONEGATIVITY EFFECTS IN CORE-LEVEL ELECTRON SPECTROSCOPES: APPLICATION TO THE HIGH TEMPERATURE SUPERCONDUCTORS

D.E. Ramaker
Chemistry Department, George Washington University, Washington, DC 20052

SUMMARY

The nature of the core level reflected in x-ray photoelectron spectroscopy, Auger electron spectroscopy, and x-ray absorption near edge structure is considered. An understanding of the effects of anion and cation electronegativity on spectra for the transition metal halides is obtained. This knowledge is applied to understand similar spectra for the high temperature superconductors.

1. INTRODUCTION

Since the discovery of the copper oxide based high temperature superconductors (HTSC) just a few years ago, a deluge of electron spectroscopic data on these materials has appeared. In spite of this great effort to elucidate their electronic structure, many basic questions remain on just how to interpret some of the data. In an effort to provide answers, some investigators have examined the more basic CuO and Cu₂O materials (1-4). In this work we shall examine some core-level electron spectroscopic data of various transition metal (TM) halides. By emphasizing the effects of anion electronegativity (X_a) on the spectra, some basic understanding can be obtained, which we then apply to the HTSC's.

This paper will consider three different reflections of a core-hole state. In Sec. 2 we examine the transition metal 2p x-ray photoelectron spectra (XPS), which reflect the initial creation of a core-hole (i.e. within the escape time of the photoelectron, typically much less than 10^{-17} sec.). Sec. 3 examines the nature of the core-level which decays in the Auger and x-ray emission processes (AES and XES), and thus reflects a more relaxed core-hole generally much later than 10^{-15} sec. after creation. Sec. 4 discusses the nature of the anion core-level in x-ray absorption near edge spectra (XANES), which reflects the unoccupied density of states after a completed response to creation of the core-hole.

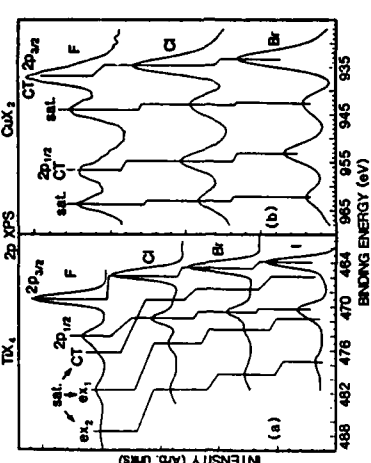
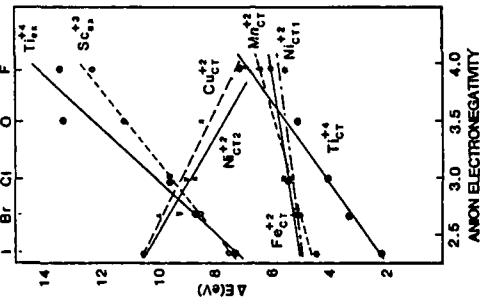


Fig. 1. Experimental main-satellite peak separation, ΔE , vs. anion electronegativity, X_a . Experimental data obtained from the following: TiX_3 (12), TiO_2 (13), $Sc(X_3)$ (9), $Cu(X_3)$ (7), $Mn(X_3)$ (10), and Ni (8). Anion electronegativity from Ref. 5. Although the data are not necessarily linear, the straight lines help to give clarity to the plot.

Fig. 2. a) Ti 2p XPS data (12) for TiX_3 complexes taken in the gas phase. Comparison with data taken in the solid phase for $TiCl_3$ (14) indicates very little differences.

b) Cu 2p XPS data for CuX_3 (7). The data for $X = Cl$ and Br have been Gaussian broadened by 3 eV to allow better comparison with that for $X = F$, which generally reveal much broader peaks.

Codes	Avail and/or
Special	A-1

1993-1
1/3/93

satellites. The excitonic satellites result from the polarization response to the core hole, and are believed to involve shakeup of an electron on the anion (9). ΔE will obviously increase with x_e for these satellites, since the binding energy of the anion valence band increases with x_e . The excitonic satellites exist only for metals near the beginning of the TM series, i.e. for Sc, Ti, and perhaps Cr, etc (9). We will not discuss them further here, but rather concentrate on the CT satellites.

It is clear from Fig. 1 that electronegativity has a dramatic effect on the separation and intensity of the CT satellite peaks. Two very different CT models exist for explaining this data. Veal and Paulikas (the VP model) (5), examining primarily the left end of the TM series, utilized a relativistic local density atomic code to calculate transition energies for atoms with different outer electronic configurations. In their work, replacement of a localized 3d electron with a more extended 4p electron simulates the movement of charge from a metal cation to a more electronegative anion (i.e. local vs. nonlocal screening). It was concluded from these calculations that the main peak arises from a locally screened final state reflecting a 2p to 3d CT response to the core hole, and the satellite from a state reflecting a more nonlocal polarization response to the core hole. Within the VP model, ΔE increases with x_e because the non-local screening response is decreasing with x_e , while the local CT response remains unchanged. The larger "chemical shift" of the satellite compared with the main peak for the TiX_2 complexes in Fig. 2, and the positive slope for all but the CuX_2 and NiX_2 materials in Fig. 1, appears to be consistent with this model.

On the other hand, Larsson (6) and Sawatzky and co-workers (the LS model) (7) utilizing an Anderson impurity Hamiltonian in a correlated cluster theory, examined the XPS data for the Cu and Ni dihalides. More recently Park et al (10) have extended the model to the Co, Fe, and Mn dihalides. The ground state is viewed as a hybridized mixture,

$$\Psi_e = A(d\alpha + \alpha d\alpha L^{-1} + \beta d\beta L^{-1}) \quad [1]$$

of the three indicated configurations, where n is the number of TM 3d electrons assuming a completely ionic compound, and L^{-1} or L^{-2} indicate the number of holes on the ligand. The diagonal energy of these configurations is given by $d\alpha = 0$, $d\beta L^{-1} = \Delta$, and $d\alpha L^{-1} = 2\Delta + U_4$ where U_4 is the effective d-d Coulomb interaction and Δ is the CT energy (7). The parameters α and β are determined by diagonalization of the 3×3 matrix with off diagonal matrix elements characterized by T , the p-d hybridization parameter. The eigenstates, $\Psi_e = A(2p^{\alpha}d^{\alpha} + \alpha' 2p^{\alpha}d^{\alpha}L^{-1} + \beta' 2p^{\beta}d^{\beta}L^{-1})$, [2]

Q is the effective core-hole, d-electron Coulomb attraction energy (7). The final state energies are obtained by diagonalization of the corresponding Hamiltonian matrix. Within the sudden approximation the XPS intensities are given by $I_e = [\langle \Psi_e | 2p^{\alpha} \Psi_e \rangle]^2$.

Assuming $U_4 = 5.0$ eV, $Q = 7.0$ eV, and $T = 2.0$ eV (parameters appropriate for Ni^{2+} when $n = 8$), Zaanen et al (8) have presented the results in Fig. 3, which gives the energy separation, ΔE , and the satellite intensities relative to the main peak, I_s/I_m , for the two possible satellites. We have also indicated in Fig. 3b, the dominant configurations in the main peak and each of the satellites. Fig. 3a also indicates the optimal Δ/T for each halide anion which provide nearly quantitative results for the NiX_2 (8). These results show that ΔE_1 is nearly constant with Δ and ΔE_2 decreases with Δ in agreement with Fig. 1 (it is assumed that Δ is proportional to x_e). Fig. 3b shows that for NiF , the main peak is primarily $2p^{\alpha}d^{\alpha}L^{-1}$ and for the remaining Ni halides, it is primarily $2p^{\beta}d^{\beta}L^{-1}$, i.e. the core hole is primarily locally screened by CT. Note that only Δ changes significantly as the halide changes.

These results can be utilized to qualitatively understand the satellites for the other TM's as well. For Cu^{2+} when $n = 9$, of course the $2p^{\alpha}d^{\alpha}L^{-1}$ configuration is no longer valid. In this case the curves for S_1 map qualitatively into M_1 and those for S_2 into S_1 (7,8). Fig. 3a shows the optimal Δ for the CuX_2 , showing that indeed ΔE then decreases with Δ in agreement with experiment (Fig. 1) (11). The results obtained by Park et al (10) for Co, Fe, and Mn are qualitatively similar to those in Fig. 3, although they included the additional configurations $cd^{\alpha}L^{-1}$ ($i=3$ to $10-n$). As we go left in the TM series, the 3d orbitals become more diffuse and shift to lower binding energy, and the lattice constant gets larger, having the effect of increasing Δ , and decreasing T and Q (10,16). Thus we move to the right in Fig. 3 as we go left in the TM series (the optimal values (10) for Δ/T and Q are shown for Mn in Fig. 3) showing that the slope of ΔE vs. x_e should shift from negative to positive in agreement with Fig. 1, and the intensity of the CT satellites should decrease in intensity (compare the Ti vs. Cu data in Fig. 2). Evidently the experimental XPS data (i.e. at least the CT satellites) for the entire TM series can be qualitatively explained by Fig. 3 and the general LS model.

Although both the VP and LS models appear to be consistent with Fig. 1, closer analysis shows the two models assign the various peaks very differently. Fig. 3 shows that as Δ/T increases, the final state forming the main peak is not the CT locally screened state, but rather the non-locally screened state. This is because as we proceed left in the TM series when Δ becomes greater than Q , the CT costs more energy than that returned from screening. This main-satellite peak reversal between Cu^{2+} and Ti^{2+} is evident from the absolute peak energies (Fig. 2), which show that the "chemical shift", due to the change in Δ ,

is largest in the CT peak; i.e. the CT satellite peak for TX_3 , the main peak for CuX_3 (7,12). It is also evident from the narrow main peak widths, which according to the LS model have primarily a $2p^1d^6$ (T^{1*}) or $2p^1d^6L^1$ (Cu^{1*}) core-hole state which offer no opportunity for multiplet splitting between the

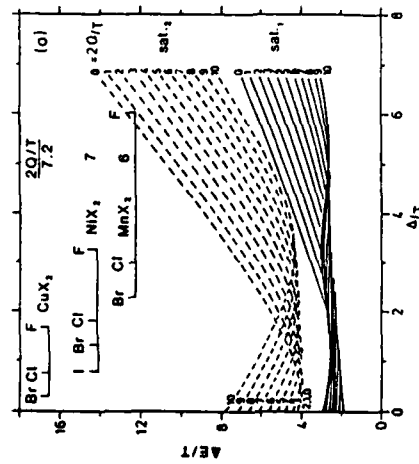


Fig. 3. Calculated results obtained by Zaanen et al. (8) utilizing the LS model for $U = 0.5$ eV, $Q = 7$ eV, and $T = 2$ eV; the parameters most appropriate for MiX_3 .

a) ΔE vs. Δ/T . The optimal Δ/T and $2Q/T$ are indicated as obtained by comparison with experimental data for CuX_3 (7), NiX_3 (8), and MnX_3 (10).

b) I/I_m vs. Δ/T . The lines for $\Delta = 0.3$, 0.7 and 1.0 Q are the points where the dominant character of the main and satellite peaks are switching the fastest with change in Δ . The dominant character within each region between these lines is indicated by the number of electrons, i , transferred to the core-hole atom for each main and satellite ($M/S_i/S_2$) feature (i.e. i in the expression $2p^1d^6L^i$). Dotted lines are for satellite 2, and solid for satellite 1.

excited electron and the core hole (9). In contrast the satellites reflect $2p^1d^6$ (T^{1*}) and $2p^1d^6$ (Cu^{1*}) states, which indeed are broadened by multiplet splitting in each case. Finally the very similar multiplet structure (such structure is often more important at the 3s and 3p levels than at the 2p levels) exhibited in the 3s and 3p core level XPS data for MnF_3 , MnO and atomic Mn (17) indicates that the CT does not occur in the primary state for these two materials either, a fact consistent with Fig. 3.

This CT main-satellite peak reversal between the left and right ends of the TM series is contrary to the VP model (5), which assumed that the main peak was always representative of the locally screened state. Of course the atomic model utilized in the VP model did not take into account the cost of the CT, and thus their basic assumption was incorrect. It seems quite ironic that although the basic VP assumption is correct for the right end of the TM series, there ΔE decreases with X_s rather than increases. We believe that the VP model therefore does not correctly interpret the XPS data anywhere, although it qualitatively is consistent with the trends in Fig. 1 for most of the TM series.

2.2 Application to the HTSC's

Recently Nepela and McKay (18) reported a remarkable correlation of T_c in the HTSC's with the electronegativity difference, ΔX between the average for all of the metal atoms, X_s , and that for the anions, X_a (see Fig. 4). They further utilized the VP model and the data in Table 1 to conclude that the Cu-O bond is becoming more ionic as T_c increases, consistent with their reported T_c vs. ΔX correlation. The data in Table 1 and the LS model indicates more correctly that the Cu-O bond is actually becoming more covalent for the HTSC's, i.e. a large Cu-O hybridization occurs and the holes or electrons are more equally shared between the Cu and the O in the HTSC's, consistent with other data (25).

If the Cu-O ionicity decreases with T_c , how can the T_c vs. ΔX correlation be explained? Newns et al (26) have suggested that ΔX does not reflect the Cu-O bond ionicity, but rather the ionicity of the remaining "counter" ions which regulate the number of holes introduced in the CuO_2 planes. It has been shown experimentally that T_c is proportional to the number of holes on the O atoms in the CuO_2 planes (27-29). Newns et al (30) have shown that this is dependent on the binding energy, E_b , relative to vacuum of the top of the O nonbonding valence band. This is because when the Fermi level drops to E_b , no additional holes will be introduced into the CuO_2 planes. Furthermore, Philips and van Vechten (31) have shown that the ionic band gap, and hence E_b , is proportional to ΔX .

3. THE CORE LEVEL IN AES AND XES

3.1 Relaxation vs. Decay

Within the sudden approximation, XPS data reflect the core-hole state shortly after its creation, say within 10^{-11} sec (5). We note that shakeup states with lifetimes significantly shorter than this will not be visible in XPS, because they relax before the photoemission is complete. This is precisely the reason why excitonic satellites are not visible in XPS for the higher TM metals (9). Well after 10^{-11} sec, the core level decays via the AES or XES process, with considerable relaxation occurring in the interim.

Evidence for relaxation of the CT shakeup satellites before Auger decay in CuX_2 is clearly evident from Figs. 2 and 5. The primary $2p^2-4p^1-1$ core-hole state decays to a dL^{-1} primary Auger final state in the $\text{Cu L}_3\text{VV}$ case and

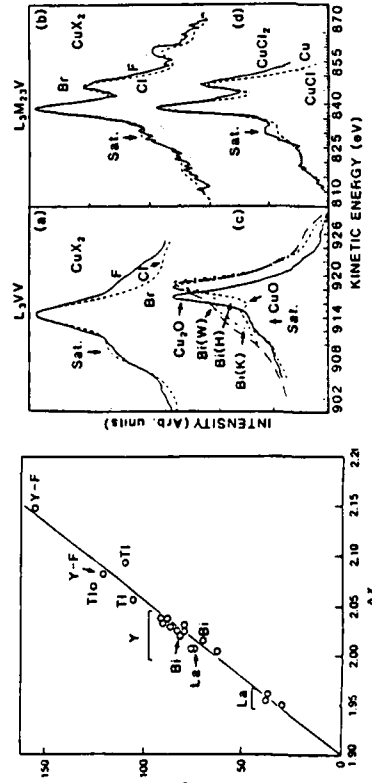


Fig. 4. Correlation reported by Nepeña and McKay (18) between T_c and $\Delta X = X_a - X$. The points have been labeled according to the basic HTSC material: $\text{La} = \text{La}-\text{Sr}-\text{CuO}$, $\text{Y} = \text{Y}(123) = \text{YM}_3\text{Cu}_2\text{O}_8$, $\text{Y} = \text{Y}(123) = \text{Y}_3\text{M}_2\text{Cu}_3\text{O}_{12}$, $\text{Ti} = \text{Ti}(2223) = \text{Ba}_3\text{Sr}_2\text{Ca}_3\text{-Cu}_2\text{O}_9$, $\text{Cu}-\text{O}$ materials, and $\text{Y}-\text{F}$ = partially fluoridized 123 materials which have been found to exhibit (albeit, nonreproducible, unpredictable, and partial) superconducting transitions at very high temperatures as indicated. The level of O is the optimal amount for each material.

a) Comparison of L_3VV Auger spectra for the CuX_2 from ref. (7). The data for $X = \text{Cl}$ and Br were shifted by -1.5 and -2.5 eV, respectively, to bring them into registry with that for $X = \text{F}$. The data for Cl and Br were Gaussian broadened by 2 eV for clearer comparison with the F data.

b) Comparison of L_3VV Auger data for the CuX_2 from ref. (7). The data for $X = \text{Cl}$ and Br were shifted by -2.75 and 3 eV for registry with the F data. The Cl and Br data were broadened by 2 eV.

c) Comparison of L_3VV Auger data for Cu_2O (7), CuO (7), and $\text{Bi}(2212)$ (data reported by Weaver (22), Hillebrecht (24), and Kohiki (21)). No shifts or broadening were performed here.

d) Comparison of L_3VV data for CuCl_2 , Cu and CuCl_3 (7). The data for Cl_2 is exactly as in b) above, and the Cu and CuCl_3 were broadened by 2 eV and placed in registry with that for CuCl_2 .

Table 1

Data showing the correlation of ΔE and I_a/I_{a0} with T_c for the HTSC's.

	CuO	$\text{La}(\text{LSCO})$	$\text{Bi}(2212)^b$	$\text{Y}(123)$	Ref.
$T_c(\text{K})$:	Not SC	40	80-85	90-95	
I_a/I_{a0}^c :	0.58 0.45 0.54	0.49 0.34	0.33 0.40-0.44 0.40	0.37 0.35 0.32 0.35	19 ^e 20 21 ^f 22 23 24
$\Delta E(\text{eV})$:	8.7 8.9	8.5 8.9	8.9	9.2 8.8 10.2	19 20 23
			9.2		24

^aAll results directly reported by author. The data varies because of different background subtractions but trends within a single investigator's results are clearly shown.
^bThe Bi 4s XPS feature may also be contributing to the satellite peak in this case (22,24).
^cRamaker has also shown that I_a/I_{a0} correlates with T_c within the $\text{Y}(123)$ samples.
^dKohiki used a variety of samples with different T_c 's.

to $d3p^1\text{L}^{-1}$ in the LaM_3V case (32,33). Auger satellites are known to arise from the $\text{L}_3\text{V}-\text{VV}$ or $\text{L}_3\text{V}-\text{M}_3\text{VV}$ processes, respectively, resulting from Coster-Kronig decay of the L_3 and L_2 core-holes and shakeoff during the initial L_3 core-hole creation. These processes can account for an Auger satellite of 0.7 relative intensity as seen in the Cu and Cu_2O lineshapes in Fig. 5 (19). It has been indicated that the CT shakeup d^6 states responsible for the XPS satellites in Cu^{+2} materials will add to this Auger satellite intensity (7,8,19). However, while Fig. 2 shows the XPS satellites to grow from 0.45 for CuBr_2 to 0.8 for CuF_2 (7), Fig. 5 shows no change in Auger satellite intensity for the CuX_2 , or even between Cu , CuO and CuO .

The above results show that clearly all CT shakeup states relax before core-hole decay (33). This is not unexpected because the shakeup excitation energy is much larger than the core-level width (34). In contrast, the additional valence-hole states resulting from Coster-Kronig decay and shakeoff do not dissipate before decay, because the extra hole is apparently bound on the local CuO_6 cluster (33).

3.2 The Nature of the Core-level Width

At least two mechanisms have been given to explain the nature of the large widths for the main Cu^{+2} 2p XPS peak. Assuming that the main peak indeed reflects predominantly the $2p^1\text{d}^1\text{L}^{-1}$ state, it has been suggested that the large width arises from the width of the anion band, i.e. from the spread of

the L hole (24,35). However, Fig. 2 shows that the width of the main 2p XPS peak increases from Br to F; however, the width of the valence band as reflected in XPS data is essentially constant for CuX₃ (7).

A second mechanism suggests that the width arises from multiplet splitting (7). The large width of the satellite is known to arise from the spread of the 2p³d⁵L⁻¹ multiplets (7). In the LS model, the mixing of the 2p³d⁵L⁻¹ and 2p³d⁶ configurations in the XPS final state, eq. (2), then causes the width of the primary peak, since the d⁶ configuration has just a single multiplet. This mechanism is consistent with the observation that the width of the main peak directly correlates with the relative intensity of the satellite as seen in Fig. 2 for the CuX₃ (7). Sacher et al (36) have also shown that the width correlates with the inductive character (or electronegativity) of the ligand for a large number of different ligands consistent with the LS model.

The Cu L₃ XES data (2,4) for CuO has a width (FWHM) of 1.7 eV, much narrower than the Cu 2p main XPS peak (3-4 eV) (1-3). One might question how the XES spectrum can be narrower than the XPS peak which reflects the initial state of the XES process. To understand this we need just to realize that in XES, the mixed 2p³d⁵/2p³d⁵L⁻¹ core-hole state decays to a mixed d⁶/d⁵L⁻¹ two-hole valence-band state. The XES spectrum is dominated by the d⁵L⁻¹ component with the d⁶ component fairly small at 12-13 eV. Therefore, consistent with Fermi's golden rule or final state rule (37), only the narrower 2p³d⁵L⁻¹ character projects onto the d⁵L⁻¹ final state. From another perspective, the entire spread of multiplets in the initial state does not contribute to the width of the XES. We note, however, that the widths of the AES peaks in Fig. 5 do increase with the widths of the XPS peaks in Fig. 2 for the CuX₃. Apparently some small component of the primary state width does project onto the AES or XES final state width.

3.3 Application to the HTSC's

Fig. 5 indicates that the L₃V₂ Auger spectrum for Bi(2212) exhibits an increased satellite intensity. This satellite intensity is also enhanced for the Y(123) materials, but it varies considerably (19,38,39), apparently because of the presence of Cu⁺ character near the sometimes O depleted surface under vacuum (40,41). Note that Fig. 5 shows the L₃V₂ Auger peak for CuO at the kinetic energy for the satellite in CuO and the HTSC's (1). This O depletion problem is particularly true of the Y(123) samples (40); but, this is much less of a problem for the Bi(2212) samples (at least the Bi samples exhibit a UPS intensity at the Fermi level) (42-51). In light of the above, this increase cannot arise from decay of the shakeup core-hole state, since it relaxes prior to the Auger decay. Furthermore, an enhanced satellite is not evident in the L₃M₂V₂ Auger spectra, and it should be visible in both if the core-hole

shakeup states are Auger decaying (33). We have suggested previously that the enhanced satellite arises from d⁵L⁻¹/d⁵L⁻¹ hybridization in the Auger 3-hole final-state (33). This hybridization is larger in the HTSC's because of the increased covalency of the HTSC's compared to CuO or the CuX₃. The difference in energy between the d⁵L⁻¹ and d⁶L⁻¹ states, as effectively reflected by the O KVV and Cu L₃V₂ Auger lineshapes, decreases from 3.1 eV in CuO (1), to 2.1 eV in CuO (1), to around 1.0 eV in Bi (2212) (22), supporting this point.

4. THE CORE LEVEL IN XANES

4.1 Excitonic Effects

The final state rule (37) generally dictates that XANES data should directly reflect the unoccupied density of states (DOS) relaxed in the presence of the core hole. Although not completely applicable for highly-correlated systems, it should be qualitatively correct for the HTSC discussed here. However, when a band is nearly full, such as the O 2p or X 3p valence bands in metal oxides or halides, the XANES excitation, p^z → 1s⁻¹p^z, completely fills these bands. In this case the XANES spectra reflects the initial unoccupied DOS without the core hole. We have termed this the initial-state/final-state rule applicable for the nearly filled VB /empty CB cases (52).

Figure 6 shows anion K edge XANES data for several TM oxides and chlorides (53-59). These data clearly show the empty O 2p/Ci 3p states in the valence band just above the Fermi level for all but CuCl, which has a filled Ci 3p valence band as expected. This initial peak has been shown to depend on the O hole density (25,60), the symmetry of the p orbitals (61,62), and the van Hove singularity (63). The peak around 531 eV in the Bi(2212) data in Fig. 7, is believed to arise from Bi-O antibonding orbitals (64-66).

Above these valence band peaks we see excitation into the O 3p/Ci 4p extended conduction bands. Here the final state rule is applicable, so that the lineshapes reflect the 3/4 P DOS in the presence of a core hole. The 3/4 P DOS has remarkably similar structure (albeit different energy scales) for all of the materials shown except for the absence of the peak around 2826 eV in the CuCl data. To understand this we need to ascertain the nature of the peak around 2826 eV at the Cl K and 533 eV at the O K edges. Multiple scattering calculations, but which do not account for the core hole, reproduce all of the structure in the spectra except for this peak, as seen for the NiO and CuO data in Fig. 6 (54,55). Those calculations which include the core hole (i.e. excitonic effects) naturally obtain this peak (53,67,68). There seems to be little doubt that this peak arises from an excitonic-like state involving the 3/4 P extended bands. Its absence in CuCl must mean that the highly polarizable filled 3d shell on the Cu atoms surrounding the Cl anion can more effectively screen the

core-hole, 4p-electron interaction, than the unfilled 3d shell in the other systems. The reason for this, however, is not entirely clear.

4.2 Application to the HTSC's

We have been unable to locate O K edge XANES data for Cu₂O. Nevertheless, we believe a similar polarization phenomenon is occurring for Cu₂O as well for some of the HTSC materials studied. Fig. 6 shows data (56) for Y (123x) with x equal to 6.98 and 6.26. Notice the much reduced feature at 533 eV in the data for x =6.26. At these very low O levels, the peak at 528.6 eV is also much reduced. At intermediate O levels (data (56) not shown in Fig. 6) the 530 eV peak decreases without reduction of the 533 eV feature. This indicates that with O reduction, the 2p DOS just above the Fermi level decreases as expected, but finally at x = 6.26, Cu¹⁺ is formed (56) as indicated by the reduced 533 eV peak. Thus the O K edge can be used to track the reduction in O 2p holes, as well as the production of Cu¹⁺.

One of the most important Hubbard parameters still not accurately known is the p-p Coulomb interaction, U_p , on the O atom (69-71). Values from 4.5 to 14 eV have been reported (1,20,72-76). The O KVV AES data rather directly indicates the two-hole binding energy which for Cu₂O is equal to $2U_p + U_p$, and UPS data directly reflect the value of the one-electron binding energy, c_p . Thus a U_p of 4.6 eV is indicated for Cu₂O (1) compared to estimates as large as 12 eV for ZnO, which also has a filled 3d shell but apparently much more core-

like and thus less polarizable (77). In CuCl, the free ion p-p interaction of 10.2 eV is reduced to 3.8 eV by polarization effects (78), again showing the large polarizability of the neighboring closed shell Cu¹⁺ ions. Similar Auger data for CuO and the HTSC's is not so easily interpreted because now the Auger final state is a 3-hole state (7,33), and the UPS final state a 2-hole state, so the values of c_p and U_p for these systems remain very uncertain (69-72, 79-81). Often, it has been assumed that U_p is the same for Cu₂O, CuO and the HTSC's (1,82).

In light of the relatively small 1s-core-hole, 3p-electron interaction experimentally deduced above for Cu₂O, one might also expect U_p to be relatively small for Cu₂O. Thus we anticipate U_p to be somewhat larger for CuO and the HTSC's, most probably around 6-8 eV (71-73).

5. CONCLUSIONS

Analysis of XPS, AES, and XANES data for TM halide and oxide data has led to the following conclusions:

1. The Larson-Szwarczyk model adequately explains the satellite structure in TM 2p XPS.
2. The satellite states visible in XPS do not produce comparable satellites in AES or XES, but rather relax before the decay process.
3. The filled 3d shells in Cu¹⁺ atoms which surround the anion in Cu⁺ halides or oxides, are uniquely strongly polarizable and thus decrease the intra-atomic anion Coulomb interactions.

Applying these findings to the HTSC's, we find the following:

1. The covalency of the Cu-O bonds increase with increasing T_c .
2. The increased LaVV Auger satellite visible for the HTSC's arises from final state mixing due to the increased covalency.
3. The O p-p coulomb interaction in CuO and the HTSC's is probably significantly larger than that for Cu₂O.
4. The O K edge XANES data can be used to track the reduction of unfilled O 2p DOS at the Fermi level as well as the production of Cu¹⁺.

ACKNOWLEDGEMENTS This work was supported in part by the Office of Naval Research. The author also wishes to thank F.L. Hutson for helping with the preparation of the figures.

REFERENCES

1. J. Ghijssen et al, Phys. Rev. 38 (1988) 11322-11330.
2. J.M. Mariot et al, Z. Phys. B - Condensed Matter 75 (1989) 1-9.
3. P. Steiner et al, Z. Phys. B - Condensed Matter 74 (1989) 173-182.
4. C.F. Hague et al, "Proc. of the Int'l. Symp. on Elect. Structure of High T_c Superconductors", Rome, 5-7 Oct. 1988, to be published.

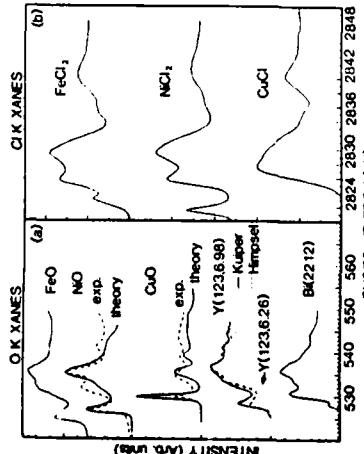


Fig. 6. a) Comparison of experimental O K XANES data for FeO (53), CuO (55), Y(123, 6.98) [Kuiper (56) and Himpel (57)], Y(123, 6.26) (56), and Bi(2212) (57). Theoretical results without the inclusion of effects from the core-hole are shown for NiO (54) and CuO (55).
 b) Comparison of experimental Cl K XANES data for FeCl₃ (58), NiCl₃ (58), and CuCl (59). The CuCl data was shifted up by 2. eV for alignment of the features above 2830 eV.

5. B.W. Veal and A.P. Paulikas, *Phys. Rev. B* 31 (1985) 5399-5416; *Phys. Rev. Lett.* 51 (1983) 1995-1998.

6. S. Larson, *Chem. Phys. Lett.* 40 (1976) 362-366.

7. G. van der Laan, C. Westra, C. Haas, and G.A. Sawatzky, *Phys. Rev. B* 23 (1981) 4369-4380.

8. J. Zaanen, C. Westra, and G.A. Sawatzky, *Phys. Rev. B* 33 (1986) 8060-8073.

9. D.K.G. deBoer, C. Haas, and G.A. Sawatzky, *Phys. Rev. B* 29 (1984) 4401-4419.

10. J. Park, S. Ryu, M. Han, and S.J. Oh, *Phys. Rev. B* 37 (1988) 10867-10875.

11. G.A. Sawatzky, Proc. of the 2nd European Conf., Veldhoven, The Netherlands, 7-9 June 1982, R. Metzelaar, H.J.M. Heijligers, and J. Schoonman (eds.), *Studies in Inorganic Chem., Elsevier, Amsterdam*, Vol. 3, pp. 3-16.

12. B. Wallbank, J.S.H.Q. Peters, D.C. Frost, and C.A. McDowell, *J. Chem. Phys.* 69 (1978) 5405-5410.

13. S.K. San, J. Riza, and J. Verbiest, *Chem. Phys. Lett.* 38 (1976) 560-564.

14. C.M. Desbuquoit, J. Riggs, and J. J. Verbiest, *J. Chem. Phys.* 79 (1983) 26-32.

15. G. Wenda, *Struct. Bonding (Berlin)* 1 (1981) 45.

16. J. Zaanen, G.A. Sawatzky, and J.W. Allen, *Phys. Rev. Lett.* 55 (1985) 418-421; *J. Magn. Magn. Mater.* 54-57 (1986) 607-611; *Can. J. Phys.* 65 (1987) 1262-1271.

17. B. Hermansseier et al., *Phys. Rev. Lett.* 61 (1988) 2592-2595.

18. D.A. Nevels and J.M. McKay, *Physica C*, to be published.

19. D.E. Ramaker et al., *Phys. Rev. B* 36 (1987) 5672-5675.

20. Z. Shen et al., *Phys. Rev. B* 36 (1987) 8414-8428; 38 (1988) 7152-7155; 39 (1989) 821-828; also to be published.

21. S. Kohiki et al., *Phys. Rev. B* 38 (1988) 7051-7053; 8868-8872; 9201-9204; 39 (1989) 4655-4698.

22. H.M. Meyer et al., *Phys. Rev. B* 38 (1988) 7144-7147; also J.H. Weaver, private communication.

23. A. Bazzotti et al., *Phys. Rev. B* 38 (1988) 6461-6469.

24. F.U. Hillebrecht et al., *Phys. Rev. B* 39 (1989) 236-242.

25. N. Nucker et al., *Phys. Rev. B* 37 (1988) 5158-5163.

26. D.M. News and P. Pattnaik, *Bull. American Phys. Soc.* 34 (1989) 561.

27. M.W. Shafer, T. Penny, and B.L. Olson, *Phys. Rev. B* 36 (1987) 4047-4050.

28. P. Steiner et al., *Z. Phys.- Condensed Matter* 69 (1988) 449-458.

29. J.B. Torrance et al., *Phys. Rev. Lett.* 61 (1988) 1127-1130.

30. D.M. News, M. Rascit, and P.C. Pattnaik, *Phys. Rev. B* 38 (1988) 6513-6530; 7033-7036.

31. J.C. Phillips, *Rev. Mod. Phys.* 42 (1970) 317-356; J.A. Van Vechten, *Phys. Rev.* 182 (1969) 891-905.

32. D.E. Ramaker, *Phys. Rev. B* 38 (1988) 11816-11819; *Chem. High T_c Superconductors II, ACS Symposium Series 377*, ACS, Washington, DC 1988, pp. 84-102.

33. D.E. Ramaker, *Phys. Rev. B* 38 (1988) 11368-11372.

34. J.W. Gadzuk and M. Sunjic, *B* 12 (1975) 524-531.

35. D.D. Sarma, *Phys. Rev. B* 37 (1988) 7948-7951.

36. E. Sacher and J.E. Kiemberg-Spieha, *Phys. Rev. B* 39 (1988) 1461-1464.

37. U. von Barth and G. Grossman, *Sol. State Commun.* 32 (1979) 645-656.

38. J.C. Fuglie et al., *Phys. Rev. B* 25 (1982) 5150-5165.

39. A. Bazzotti et al., *Phys. Rev. B* 36 (1987) 8285-8287.

40. R.S. List et al., *Phys. Rev. B* 38 (1988) 11956-11969.

41. T. Takahashi et al., *Phys. Rev. B* 37 (1988) 9788-9795.

42. Y. Chang et al., *Phys. Rev. B* 39 (1988) 4740-4743.

43. J.M. Imer et al., *Phys. Rev. Lett.* 62 (1989) 336-339.

44. T. Takahashi et al., *Phys. Rev. B* 39 (1989) 6636-6639.

45. D.E. Morris et al., *Phys. Rev. B* 39 (1989) 6612-6614.

46. D.M. Hill et al., *Phys. Rev. B* 38 (1988) 11331-11336.

47. J.N. Tariscon et al., *Phys. Rev. B* 38 (1988) 8895-8892.

TECHNICAL REPORT DISTRIBUTION LIST, GENERAL

No. Copies	No. Copies		
Office of Naval Research Chemistry Division, Code 1113 800 North Quincy Street Arlington, VA 22217-5000	3	Dr. Ronald L. Atkins Chemistry Division (Code 385) Naval Weapons Center China Lake, CA 93555-6001	1
Commanding Officer Naval Weapons Support Center Attn: Dr. Bernard E. Douda Crane, IN 47522-5050	1	Chief of Naval Research Special Assistant for Marine Corps Matters Code 00MC	1
Dr. Richard W. Drisko Naval Civil Engineering Laboratory Code 152 Port Buenos, California 93043	1	800 North Quincy Street Arlington, VA 22217-5000	
Defense Technical Information Center Building 5, Cameron Station Alexandria, Virginia 22314	2	Dr. Bernadette Eichinger Naval Ship Systems Engineering Station Code 053 Philadelphia Naval Base Philadelphia, PA 19112	1
David Taylor Research Center Dr. Eugene C. Fischer Annapolis, MD 21402-5067	1	Dr. Sachio Yamamoto Naval Ocean Systems Center Code 52 San Diego, CA 92152-5000	1
Dr. James S. Murday Chemistry Division, Code 6100 Naval Research Laboratory Washington, D.C. 20375-5000	1	David Taylor Research Center Dr. Harold H. Siegeman Annapolis, MD 21402-5067 ATTN: Code 283	1